



Bcl-2 inhibitor upconverted upconversion nanophotosensitizers to overcome the photodynamic therapy resistance of cancer through adjuvant intervention strategy



Xiaomin Liu ^a, Zhongqi Fan ^b, Li Zhang ^b, Zheng Jin ^c, Dongmei Yan ^c, Youlin Zhang ^a, Xiaodan Li ^b, Langping Tu ^a, Bin Xue ^a, Yulei Chang ^{a, **}, Hong Zhang ^{d, ***}, Xianggui Kong ^{a, *}

^a State Key Laboratory of Luminescence and Applications, Changchun Institute of Optics, Fine Mechanics and Physics, Chinese Academy of Sciences, 130033, Changchun, Jilin, China

^b The First Hospital, Jilin University, Changchun, Jilin, 130021, China

^c Department of Immunology, College of Basic Medical Sciences, Jilin University, Changchun, Jilin, 130021, China

^d Van't Hoff Institute for Molecular Sciences, University of Amsterdam, Science Park 904, 1098 XH, Amsterdam, The Netherlands

ARTICLE INFO

Article history:

Received 3 July 2017

Received in revised form

7 August 2017

Accepted 8 August 2017

Available online 11 August 2017

Keywords:

PDT resistance

Upconversion nanoparticle

Inhibitor

Tumor microenvironment

Antioxidant enzyme

ABSTRACT

Similar to many other anticancer therapies, photodynamic therapy (PDT) also suffers from the intrinsic cancer resistance mediated by cell survival pathways. These survival pathways are regulated by various proteins, among which anti-apoptotic protein Bcl-2 plays an important role in regulation of programmed cell death and has been proved to involve in protecting against oxidative stimuli. Confronted by this challenge, we propose and validate here a novel upconversion photosensitizing nanoplatfrom which enables significant reduction of cancer resistance and improve PDT efficacy. The upconversion nanophotosensitizer contains the photosensitizing molecules - Zinc phthalocyanine (ZnPc) and Bcl-2 inhibitor - ABT737 small molecules, denoted as ABT737@ZnPc-UCNPs. ABT737 molecules were encapsulated, in a pH sensitive way, into the nanoplatfrom through Poly (ethylene glycol)-Poly (L-histidine) diblock copolymers (PEG-*b*-PHis). This nanosystem exhibits the superiority of sensitizing tumor cells for PDT through adjuvant intervention strategy. Upon reaching to lysosomes, the acidic environment changes the solubility of PEG-*b*-PHis, resulting in the burst-release of ABT737 molecules which deplete the Bcl-2 level in tumor cells and leave the tumor cells out from the protection of anti-apoptotic survival pathway in advance. Owing to the sensitization effect of ABT737@ZnPc-UCNPs, the PDT therapeutic efficiency of cancer cells can be significantly potentiated *in vitro* and *in vivo*.

© 2017 Published by Elsevier Ltd.

1. Introduction

Photodynamic therapy (PDT) has been well-accepted in clinics as a prospective alternative to conventional anticancer therapies such as surgery, radiotherapy and chemotherapy. PDT entails the systemic administration of a photosensitizer (PS), its accumulation in tumor tissue, and subsequent irradiation of the PS-replete tumor, leading to the localized photoproduction of reactive oxygen species

(ROS). The resulting oxidative damage causes tumor cell death, vascular shutdown, and an anti-tumor immune response that ultimately culminates in the removal of tumor [1]. However, the ROS generated by PDT also sets off a stress response, as part of cell survival mechanism that contributes to cancer cells responding to PDT-induced oxidative stress and cell injury [2]. For example, antioxidant response can be triggered by activation of redox sensitive transcription factors, resulting in an increase in detoxifying and antioxidant enzymes. The heat shock response can be induced by over expression of heat shock proteins, leading to a decrease of active apoptosomes. Proteotoxic stress is set off by activation of anti-apoptotic pathways, etc. [3] These survival mechanisms are perceived as causing certain types of cancer insusceptible to PDT and making tumor microenvironment contribute to tumor survival,

* Corresponding author.

** Corresponding author.

*** Corresponding author.

E-mail addresses: yuleichang@ciomp.ac.cn (Y. Chang), h.zhang@uva.nl (H. Zhang), xgkong14@ciomp.ac.cn (X. Kong).

resulting in therapeutic resistance. Rationally, if the generation of those molecules involved in PDT resistance are inhibited, the quality of therapy can be improved greatly.

Proteins in the Bcl-2 family mainly regulate programmed cell death, and the anti-apoptotic members, such as Bcl-XL and Bcl-2, are overexpressed in many cancers and contribute to tumor initiation, progression and resistance to therapy. Numerous studies have demonstrated that tumors upregulate antiapoptotic proteins as an adaptive response against oxidative stress [4,5]. Among many antiapoptotic proteins, Bcl-2 is the most typical one located mainly in the outer mitochondrial membrane [6]. Hochman et al. demonstrated higher oxidative damage and susceptibility to ROS in brains of Bcl-2 deficient mice compared with that of wild-type mice [7]. Overexpression of Bcl-2 shifts the cellular redox potential to a more reduced state, thus presents relatively high antioxidant capacity, facilitating cancer cells' survival from oxidative stimuli and lowering the sensitivity to ROS [8].

ABT737 molecules, an inhibitor of Bcl-2 proteins, could bind to the hydrophobic groove of anti-apoptotic proteins, preventing the dimerization of anti-apoptotic proteins with pro-apoptotic. The released pro-apoptotic proteins (like Bax and Bak) oligomerize on the mitochondrial outer membrane and permeabilize it, resulting in the release of apoptogenic proteins that mediate cellular demolition [9]. There has been several reports on the application of anti-apoptotic protein Bcl-2 inhibitors to sensitize tumor cells to PDT-induced damage [10,11]. However, the inhibitors and photosensitizers were injected separately in most cases, it is difficult to realize the simultaneous optimal accumulation of both inhibitors and photosensitizers in tumor cells, especially for *in vivo* treatment. Moreover, the Bcl-2 inhibitors are lack of tumor targeting. It should be noted that the anti-apoptotic protein Bcl-2 expressed not only in tumor cells but also in normal cell. How to inhibit the expression level of Bcl-2 in tumor cell, rather than affecting the protection role of Bcl-2 in normal cells, is thus a big issue. On the other hand, recent advances in nanotechnology and nanomedicine have provided some efficient strategies to deal with the challenges in traditional PDT, like (i) the limited tissue penetration depth of ultraviolet to visible excitation light, which confines traditional PDT to superficial tumors; (ii) the very short lifetime and limited diffuse distance of ROS, which need specific delivery of photosensitizers to sub-cellular organelles for exerting effective toxicity; (iii) the hypoxic tumors exhibit less effective to PDT treatment, etc. [12–17] However, little research performed on PDT therapeutic resistance and the underlying biology.

Herein, we propose an intelligent NIR laser-triggered nanophotosensitizer for relieving the resistance of cancer to PDT based on the important role of Bcl-2 protein involved in PDT resistance as well as the unique properties of upconversion nanoparticles. Upconversion nanoparticles enable deeper tissue penetration due to near-infrared (NIR) excitation, negligible autofluorescence background and enhanced photostability [18–22]. The novel nanophotosensitizer integrates Bcl-2 inhibitor - ABT737 molecules and the photosensitizing molecules - Zinc phthalocyanine (ZnPc) into a single upconversion nanocarrier, denoted as ABT737@ZnPc-UCNP. Specifically, encapsulation of ABT737 molecules into the nanocomplex is realized through pH-sensitive Poly (ethylene glycol)-Poly (ι -histidine) diblock copolymers (PEG-*b*-PHis), which could attenuate the *in vivo* toxicity and enhance the tumor accumulation of ABT737. The dynamic subcellular distribution of ABT737@ZnPc-UCNPs demonstrates their internalization proceeding from endolysosome to cytosol, and then to mitochondria. Once the nanocomplex reaches lysosomes, the acidic environment changes the solubility of the outer functional polymer PEG-*b*-PHis resulting in the burst-release of ABT737 molecules which inhibit anti-apoptotic protein Bcl-2 and the cancer cells are thus more

sensitive to PDT (Fig. 1a). *In vitro* and *in vivo* studies were carried out to monitor the susceptibility to ROS, the mechanism of cancer cell death, the tumor angiogenesis as well as the levels of antioxidant enzymes in PDT mediated by ABT737@ZnPc-UCNPs and the control group of ZnPc-UCNPs. Our results indicate that the ABT737@ZnPc-UCNPs can significantly potentiate PDT efficiency through preventing tumor cells evasion of apoptosis internally and making the tumor microenvironment susceptible to oxidative stimuli externally, which offers a potentially new adjuvant intervention strategy to improve PDT effect.

2. Materials and methods

2.1. Materials

YCl₃·6H₂O (99.9%), YbCl₃·6H₂O (99.9%), ErCl₃·6H₂O (99.9%), NaOH (98%), NH₄F (98%), 1-octadecene (90%) and Oleylamine (OM) were purchased from Sigma-Aldrich. Fluoresceinyl cypridina luciferin analogue (FCLA) was purchased from Tokyo Kasei Kogyo Co. Tokyo, Japan. ABT737 was purchased from Selleck Chemicals (Houston, TX). All chemicals were used as received without further purification. 2, 9, 16, 23-tetracarboxylic Zinc phthalocyanine and poly (ethylene glycol)-poly (ι -histidine) (PEG-PHis) diblock copolymer were synthesized according to the references. [24].

2.2. Characterization

The transmission electron microscopy (TEM) was performed on a Tecnai G2 F20 S-TWIN D573 electron microscope operated at 300 kV TEM. Ultraviolet–visible (UV–VIS) absorption was measured by a UV-3101 spectrophotometer at room temperature. The fluorescent emission spectra were measured by a Hitachi F-4500 fluorescence Spectro fluorimeter at room temperature. Cell imaging was collected by using a modified confocal laser scanning microscope under excitation of 980 nm laser light (CLSM, Nikon C2 microscope with a CCD camera).

2.3. Ligand exchange assembly of UCNPs with ZnPc(COOH)₄

The hydrophobic UCNPs solution (~10 mg, purified and dispersed in 2 mL of cyclohexane) was mixed with the different amounts of ZnPc(COOH)₄. After adding 2 mL Tetrahydrofuran (THF), the solution was stirred vigorously over 24 h at 30 °C. UCNPs-ZnPc nanocomplex was then centrifuged and washed with acetone to remove any unreacted ZnPc(COOH)₄. The obtained nanocomposites were redispersed in DMSO for further use.

2.4. Surface functionalization with PEG-PHis and ABT737

The number average molecular weight (Mn) of PEG-PHis is 4193 (PEG2000-PHis2193) and the polydispersity index (PDI) is 1.20. NMR and size exclusion chromatography (SEC) charts were given in Fig. S1. Briefly, 6 mg PEG-PHis, 0.1 mg ABT737, and 0.3 mg UCNPs-ZnPc were mixed with 2 mL of Dimethyl Sulphoxide (DMSO), followed by the addition of 2 mL pH = 9.2 buffer. The solution was then transferred to a bag (cut-off 3500 MW) for dialysis against pH = 9.2 buffer for 2 days. Subsequently, the as-prepared micelles were purified through centrifugation to remove the excess free polymer and ABT737, then filtered with a 0.22 μ m filter. Due to hydrophobic-hydrophobic interactions, this strategy can produce a stable polymer shell on UCNPs-ZnPc and convenient for encapsulating the ABT737 molecules in the hydrophobic shell.

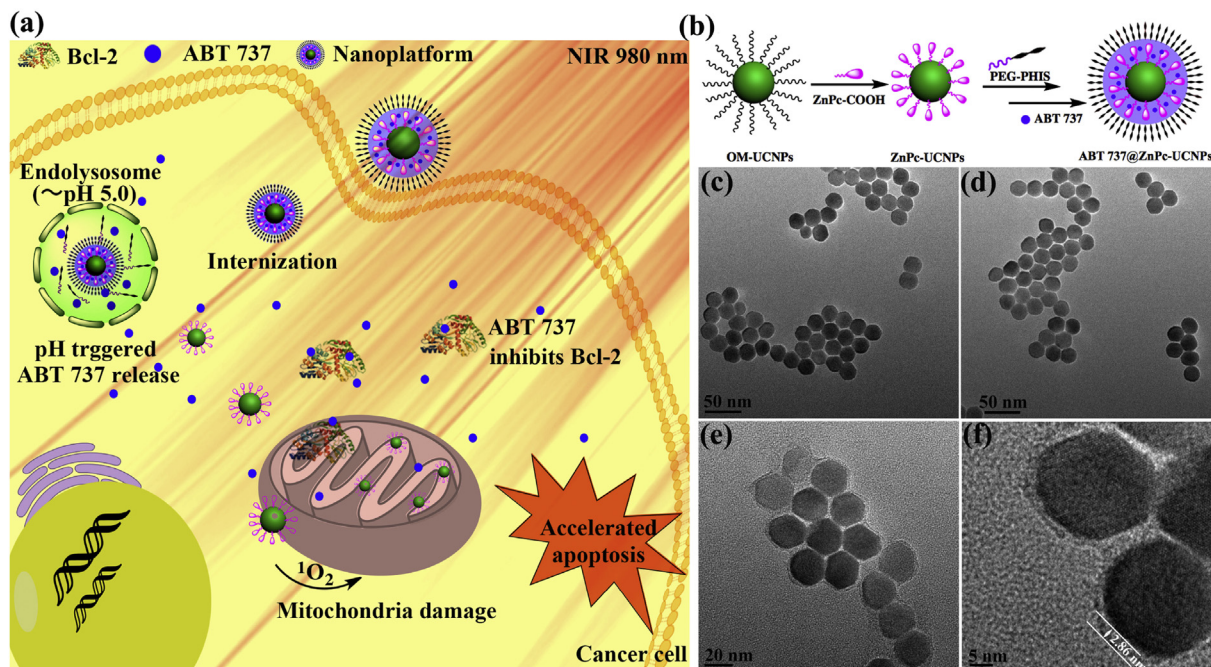


Fig. 1. (a) Conceptual graphical overview of the constructed ABT737@ZnPc-UCNPs nanophotosensitizer potentiating PDT efficiency through inhibition anti-apoptosis in cancer cells. (b) The construction of ABT737@ZnPc-UCNPs nanophotosensitizer. (c) TEM image of oleylamine (OM)-capped $\text{NaYF}_4: \text{Yb}^{3+}, \text{Er}^{3+}$ UCNPs. (d) TEM image of ZnPc-UCNPs nanocomplex. (e) and (f) TEM image of ABT737@ZnPc-UCNPs nanophotosensitizer after staining with phosphotungstic acid to enhance the contrast and the visualization of the polymer shells, which was measured to be about 2.86 nm.

2.5. Loading capacity and ABT737 release profiles

The standard absorption curve of $\text{ZnPc}(\text{COOH})_4$ in DMSO solution was made with the absorption range from 0.3 to 0.6. UCNPs of 10 mg were mixed with various amounts of $\text{ZnPc}(\text{COOH})_4$. After removing free $\text{ZnPc}(\text{COOH})_4$ by centrifugation and washing, a certain amount of UCNPs-ZnPc was diluted by DMSO, UV–VIS absorption spectra of UCNPs-ZnPc were recorded. UV–VIS absorption spectra of UCNPs were also measured as background in the same way. The $\text{ZnPc}(\text{COOH})_4$ loading capacity = [amount of $\text{ZnPc}(\text{COOH})_4$ in the UCNPs (g)]/[amount of UCNPs-ZnPc (g)] \times 100. ABT737 loading capacity was measured in the similar way. The release of ABT737 from the nanocomplex was evaluated by equilibrium dialysis method against different pH buffer and monitored by UV–VIS spectrometry at 431 nm to determine the rate and cumulative release amount of ABT737. Singlet oxygen was measured according to the references. [26].

2.6. Cell viability assay

Cell viability was measured according to the standard MTT (Sigma Aldrich) assay method (see supporting information for details).

2.7. Immunostaining

For investigation of intracellular distribution dynamics of nanophotosensitizer, cells were incubated with 20 $\mu\text{g}/\text{mL}$ ABT737@UCNPs-ZnPc for different times (1 h, 6 h, 10 h, and 24 h) at 37 $^\circ\text{C}$ and washed with PBS three times. we used 300 nM MitoTracker Green for 40 min to stain the mitochondrion, 500 nM LysoTracker Red for 1 h to stain lysosome at 37 $^\circ\text{C}$ following by gently washed with PBS three times. Upconversion fluorescence and subcellular organelle imaging were then performed using a Nikon confocal microscope. Apoptosis was evaluated by DAPI that

specifically targets nucleus. Cells were incubated with 20 $\mu\text{g}/\text{mL}$ UCNPs-ZnPc or ABT737@ZnPc-UCNPs for 24 h and washed thrice with PBS. After 10 min exposure of 980 nm light at 0.4 W/cm^2 , the cells were allowed to incubate for an additional 24 h to induce apoptosis. Cells were fixed by 4% paraformaldehyde and stained by DAPI (0.1 mg/mL) for 10 min. The samples were washed by PBS 3 times, followed by observation with Nikon confocal microscope. For the flow cytometry analysis, they were trypsinised and stained by Annexin V-FITC and propidiumiodide (AnnexinV Apoptosis Detection KitII, BD Biosciences, SanDiego, CA) to measure the cells experiencing apoptosis. The process was executed using FACScan flow cytometer (Becton Dickinson, Franklin Lakes, NJ). For JC-1 assay, cells were incubated with 20 $\mu\text{g}/\text{mL}$ UCNPs-ZnPc or ABT737@ZnPc-UCNPs for 24 h and washed thrice with PBS. After 10 min exposure of 980 nm light at 0.4 W/cm^2 , the cells were allowed to incubate for an additional 24 h to induce apoptosis. The cells were then stained by JC-1, washed, and taken for imaging on a Nikon confocal microscope. Fluorescence of J-monomer and J-aggregate could be detected simultaneously under 488 nm excitation. In order to investigate the morphology of mitochondrion, cells were incubated with 20 $\mu\text{g}/\text{mL}$ UCNPs-ZnPc or ABT737@ZnPc-UCNPs for various time (12 and 24 h) and washed thrice with PBS. After 10 min exposure of 980 nm light at 0.4 W/cm^2 , the cells were allowed to incubate for an additional 24 h to induce apoptosis. The cells were stained by 250 nM MitoTracker Red, washed, and taken for imaging on a Nikon confocal microscope.

2.8. Western blot and others

Antibodies were purchased as the following, and suppliers and the dilution ratio were also marked: rabbit monoclonal anti-Bak (1:1000), rabbit monoclonal anti-Bcl-2 (1:1000), rabbit monoclonal anti caspase-3 (1:500) mouse monoclonal anti-cytochrome C (1:200), horseradish peroxidase-labeled Goat Anti-Mouse secondary antibody (1:1000), horseradish peroxidase-labeled Goat Anti-

Rabbit (1:1000) secondary antibody were purchased from Beyotime Biotechnology, Shanghai, China. See [supporting information](#) for the details. In vivo PDT, immunohistochemical analysis and antioxidant enzymes analysis. See details in [Supporting information](#).

3. Results and discussion

3.1. Synthesis and characterization of the nanophotosensitizer

The construction of ABT737@ZnPc-UCNPs is illustrated in [Fig. 1b](#). The oleylamine (OM)-capped NaYF₄: 30% Yb³⁺, 2% Er³⁺ nanocrystals were prepared via a solvothermal method [23] and used as the donor. 30% Yb³⁺ doping concentration was used in this case, instead of 20% Yb³⁺ generally applied in the current studies, to increase the red upconversion luminescence (UCL) at 650 nm (the upconversion luminescence spectrum was given in [Fig. S2](#)), facilitating the maximum spectra overlap integral between the donor NaYF₄: 30% Yb³⁺, 2% Er³⁺ nanocrystals and the acceptor ZnPc(COOH)₄ molecules. The transmission electron microscopy (TEM) in [Fig. 1c](#) ensures that the OM-capped NaYF₄: 30% Yb³⁺, 2% Er³⁺ UCNPs possessed uniform morphology with sizes around 26 ± 2 nm. A ligand exchange strategy, where the carboxyl groups of ZnPc(COOH)₄ could readily replace the original oleylamine ligands and coordinate to Ln³⁺, was applied to construct the ZnPc-UCNPs nanophotosensitizer in order to shorten the energy transfer distance between the UCNPs and the surface anchored ZnPc. Such a process did not alter the size and morphology of UCNPs, as is shown in [Fig. 1c](#) and d. PEG-b-PHis polymers (the characterization of the polymer was given in [Fig. S1](#)) were subsequently used to stabilize ZnPc-UCNPs in biological media due to hydrophobic-hydrophobic interactions. During this process, ABT737 molecules could also be physically encapsulated into the hydrophobic layer of the polymer to form the ABT737@ZnPc-UCNPs. The PEG-b-PHis confers the nanophotosensitizer's response to local pH changes. The stability of PEG-b-PHis depends on the hydrophobicity. At lower pH, protonation of the amine group makes the hydrophobic imidazole group in the histidine repeat unit into hydrophilic [24]. The critical micelle concentration (CMC) of nanoparticles was 15.6 µg/mL above pH7.4, which prevented the nanophotosensitizer from dissociation upon dilution in the blood stream *in vivo*. The CMC increased significantly on decreasing the pH below 7.2. Moreover, when pH dropped to 5, the CMC could not be detected. As indicated in [Fig. S3](#), the maximum of the cumulative release of ABT737 in ABT737@ZnPc-UCNPs was observed at pH 5. Therefore,

when the ABT737@ZnPc-UCNPs nanophotosensitizers entered the acidic environment, such as endo-/lysosome, the hydrophobic layer of the polymer became hydrophilic, swelling and fracture, leading to the release of ABT737 molecules. After encapsulation, the average size of the particles was measured by TEM to be 29 nm, which is in good consistency with the diameter of the original OM-capped nanoparticles. However, the dynamic light scattering (DLS) analysis showed an increase in the size of the nanocomplex after encapsulation (see [Fig. S4](#)). The nanoparticles grew to approximately 70 nm, which can be attributed to the addition of the organic shell to the inorganic core. The organic polymer shell could be directly visualized using TEM after staining the sample with phosphotungstic acid, which increased the contrast and displayed the shells as halos around the nanoparticles ([Fig. 1e](#)). The polymer shell thickness was thus determined about 2.86 nm ([Fig. 1f](#)). It should be noted that during TEM sample preparation, the organic portion will contract around the nanoparticles as drying occurs resulting in an organic layer that is not as large as measured using DLS, which has also been observed by other groups [25].

The successful formation of ABT737@ZnPc-UCNPs was also evidenced by the absorption spectrum ([Fig. S5](#)). Encapsulated by polymer, the ABT737@ZnPc-UCNPs were transferred from DMSO to aqueous phase, where the peak at 417 nm is attributed to ABT737 molecules, and the one at 709 nm comes from ZnPc which is slightly red-shifted referenced to that of ZnPc(COOH)₄ at 702 nm in DMSO, ascribing to the phase transfer resulting in closer proximity between ZnPc(COOH)₄ molecules. The optimal loading capacity of ZnPc(COOH)₄ and ABT737 molecules in ABT737@ZnPc-UCNP nanocomposites was determined as 4.37 wt% and 7.25 wt%, respectively (See details in [Figs. S6 and S7](#) and experimental section). The releasing behaviors of ABT737@ZnPc-UCNP nanocomposites in two different buffer solutions (pH 7.4 and 5.5) were studied and the results were provided in [Fig. 2a](#). A typical two-phase-release profile was observed in both solutions i.e. a relatively rapid release followed by a sustained and slow release over a prolonged time up to several hours. The time constants are, however, pH dependent. ABT737-release from ABT737@ZnPc-UCNPs nanocomposites at pH 5.5 is much faster which is mainly due to the increased protonation of the polymer at lower pH. In contrast, the ZnPc molecules on the surface of UCNPs were quite stable in pH 5.5 buffer solution - as high as 96.8% ZnPc survived after 24 h stirring ([Fig. S8](#)). We further examined the production of ¹O₂ from ABT737@ZnPc-UCNPs in live cells using 2,7-dichlorofluorescein diacetate (DCFH-DA). DCFH-DA distributes in live cells and emits bright green fluorescence in the presence of ¹O₂ [26]. Mouse lewis

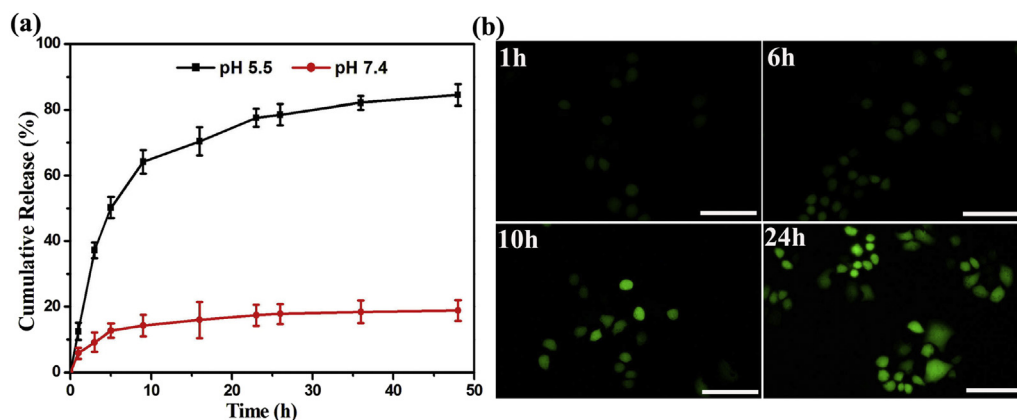


Fig. 2. (a) The release curve of ABT737@ZnPc-UCNPs nanophotosensitizer at different pH values. (b) Detection of intracellular reactive oxygen production by DCFH-DA staining in LLC cells incubated with ABT737@ZnPc-UCNPs at different times following by 980 nm laser irradiation (0.4 W/cm² for 10 min). Scale bar, 50 µm.

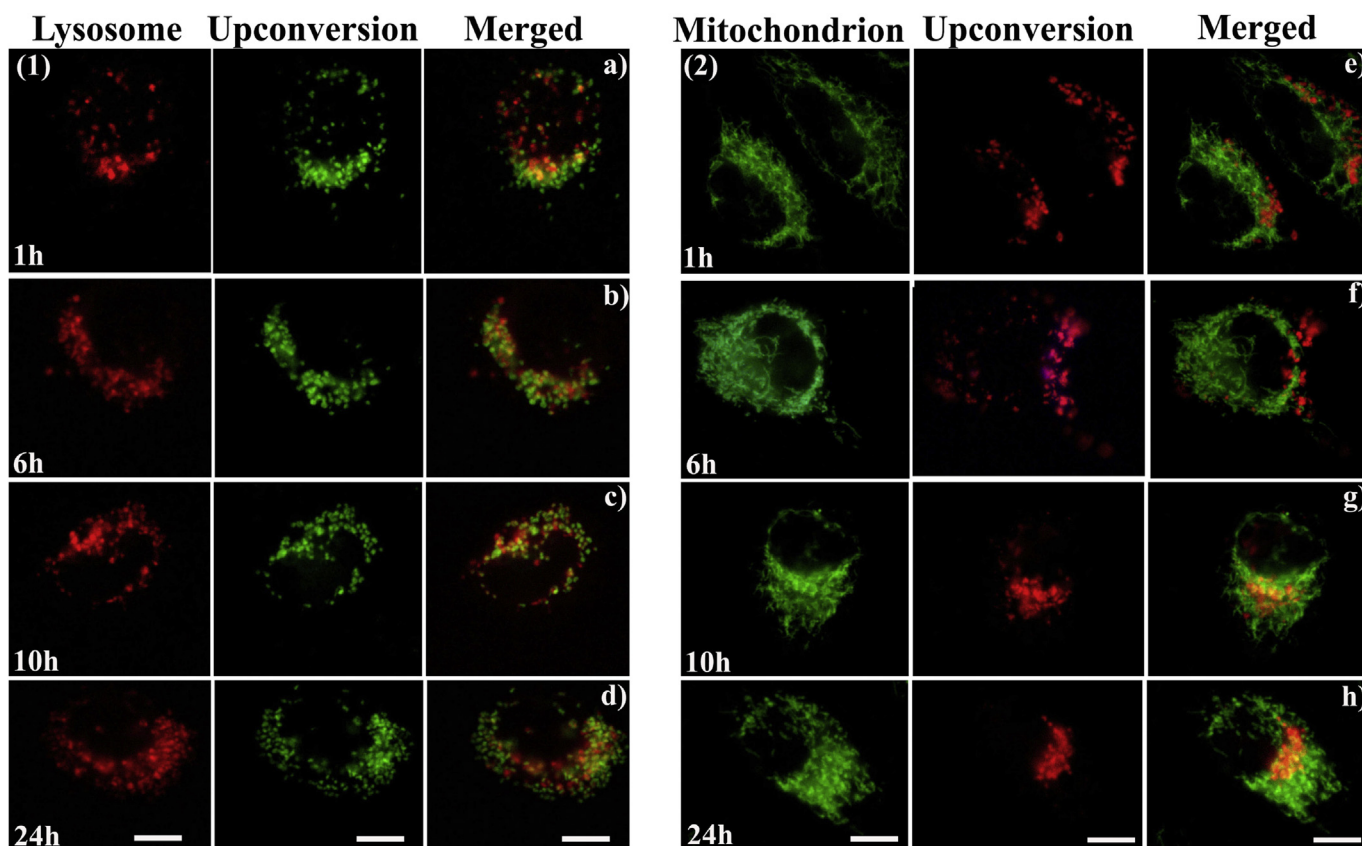


Fig. 3. (a) Cell uptake and intracellular location of ABT737@ZnPc-UCNPs nanophotosensitizer at different times. Scale bar, 10 μm .

lung carcinoma (LLC) cells were incubated with the same amount of ABT737@ZnPc-UCNPs at different times followed by 980 laser irradiation (0.4 W/cm² for 10 min). The oxidatively stressed cells showed green fluorescence (Fig. 2b), indicating a significant increase of ¹O₂ after 24 h incubation.

3.2. Intracellular distribution dynamics of nanophotosensitizer

To comprehend the mechanism underlying this increase, the internalization and organelle localization process of the ABT737@ZnPc-UCNPs were monitored. We have incubated the cells with ABT737@ZnPc-UCNPs at different times followed by treatment with mitotracker and lysotracker, respectively. Considering that the ABT737@ZnPc-UCNPs could exhibit red and green luminescence under 980 nm excitation, the potential colocalization between ABT737@ZnPc-UCNPs and lysosome (or mitochondrion) should yield a yellow/orange overlap when the images are merged. As indicated in Fig. 3, confocal images provide spatial and temporal information about the intracellular distribution of the ABT737@ZnPc-UCNPs, which occurred in a time-dependent manner. ABT737@ZnPc-UCNPs were internalized into mouse LLC cells and then gradually trafficked to endosomes/lysosomes at 1, 6 and 10 h (Fig. 3a, b and c). Within 24 h, most ABT737@ZnPc-UCNPs gradually entered and filled the lysosomes, as evidenced by the more colocalization (Fig. 3c and d, the quantitatively analysis of colocalization was given in Fig. S9). Whereas red emission of ABT737@ZnPc-UCNPs presented diffused pattern at the first 6 h exhibiting no obvious overlap with green mitotracker (Fig. 3e and f). At 10 h, some appeared in mitochondria in a punctuated luminescence pattern (Fig. 3g) and the number increased gradually. At 24 h, the ABT737@ZnPc-UCNPs exhibited aggregation and yellow

color was clearly observed in mitochondria (Fig. 3h and Fig. S9). Based on these results we can draw a picture that ABT737@ZnPc-UCNPs locate at the cell membrane at the beginning and then enter the cell to form endosomes, which are then mixed together with lysosomes. The endosomal/lysosomes membrane is fractured by the proton-sponge effect of imidazole groups [27], facilitating the release of ABT737 molecules and ZnPc-UCNPs nanophotosensitizers. The released ABT737 molecules move to mitochondrial, endoplasmic reticulum, and nuclear membranes to inhibit Bcl-2 [28], whereas ZnPc-UCNPs migrate to mitochondria as internalization proceeds.

3.3. The mechanism of ABT737@ZnPc-UCNPs sensitized cancer cells to PDT in vitro

3.3.1. In vitro PDT

Based on the information of intracellular distribution, cytotoxicity of ZnPc-UCNPs and ABT737@ZnPc-UCNPs against LLC cancer cells was evaluated by MTT assay after 24 h incubation. Dark toxicity, as a control, was also evaluated. No significant decrease in viability was observed with ZnPc-UCNPs or ABT737@ZnPc-UCNPs, as shown in Fig. S10a. When LLC cancer cells were exposed to NIR light at a relatively low dosage of 0.4 W/cm² for 10 min, the cell viability (shown in Fig. 4a) in both cases decreased, which was more profound with higher drug dosage. For example at 120 $\mu\text{g}/\text{mL}$ concentration, ZnPc-UCNPs and ABT737@ZnPc-UCNPs reduced cell viability up to 57 and 89% respectively, indicating a robust therapeutic effect of ABT737@ZnPc-UCNPs as compared to that of ZnPc-UCNPs. Whereas the same amount of ABT737 alone did not show any toxic effect regardless of NIR light irradiation or not (Fig. S10b).

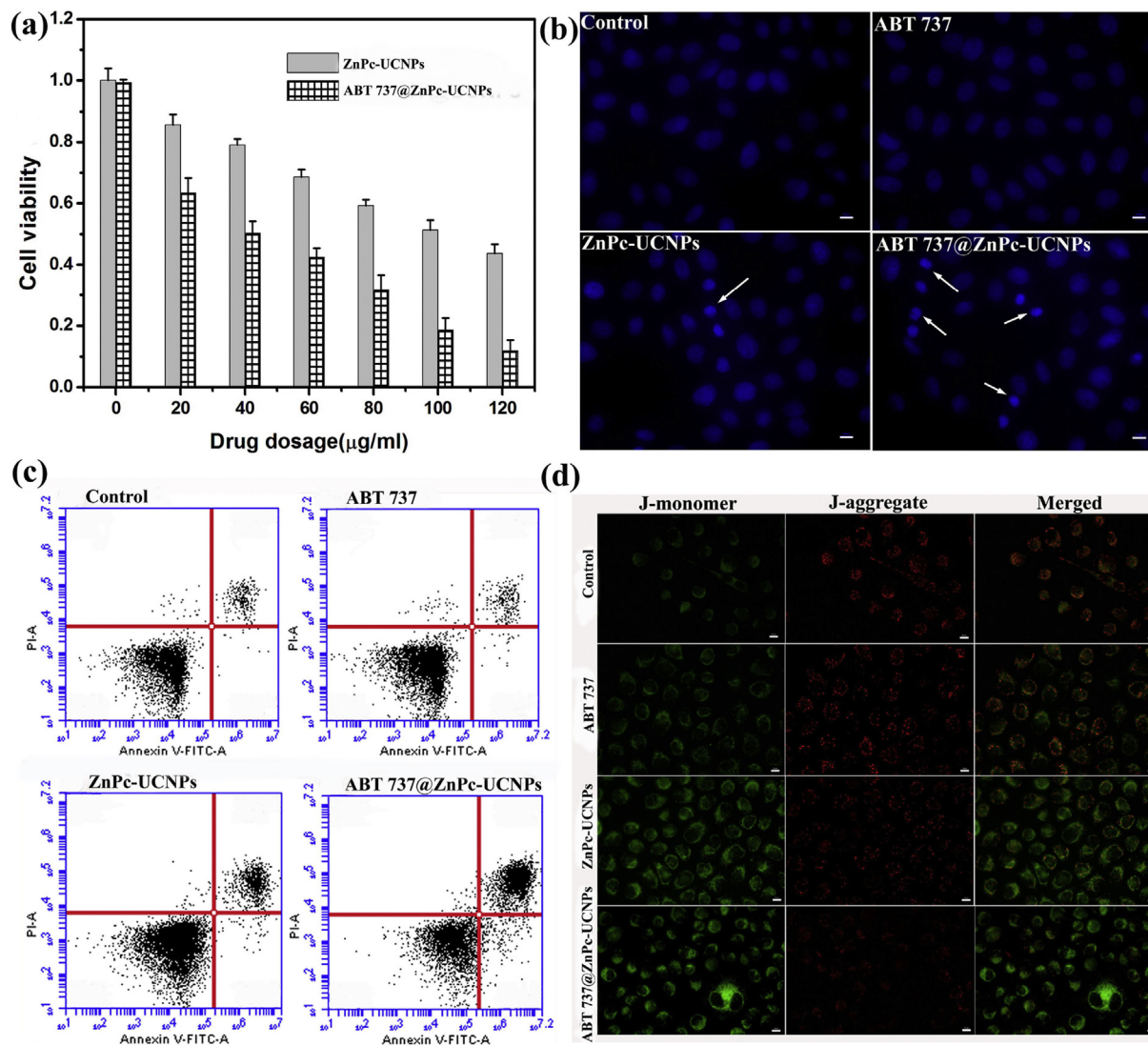


Fig. 4. (a) The cell viability of ABT737@ZnPc-UCNPs mediated PDT. Data was shown as mean \pm SD, $n = 3$. (b) DAPI was used to stain the cells. The nuclear morphology was observed by fluorescence microscopy. Bar: 10 μm . Arrows represent apoptotic nuclear changes. (c) Cells were stained by Annexin V and PI, and analyzed by FACS. ABT737@ZnPc-UCNPs induced apoptosis in 54.1% cells, much higher than 19.9% of ZnPc-UCNPs group, 5.8% of ABT737 group and 5.5% of the control group. (d) Confocal imaging of LLC cells under 488 nm excitation. The cells were incubated with ABT737@ZnPc-UCNPs for 24 h at 37 $^{\circ}\text{C}$, irradiated by a 980 nm laser, and then stained by 10 $\mu\text{g}/\text{mL}$ JC-1. J-monomer and J-aggregate were detected in the green (500–530 nm) and red (550–600 nm) channels, respectively. Scale bar: 10 μm . (For interpretation of the references to colour in this figure legend, the reader is referred to the web version of this article.)

3.3.2. ABT 737@ZnPc-UCNPs intensified the cell apoptosis

Cell death in PDT could follow various pathways including apoptosis, necrosis, and autophagy-associated cell death. Metalated phthalocyanines were proved to be mainly involved in apoptotic cell death pathways, resulting in more effective cell death than other previous generation photosensitizers [29]. The effect of ABT737@ZnPc-UCNPs on apoptotic death in LLC cells was in the first place assessed by DAPI stain. DAPI reagent can be easily assimilated by cells in the initial stages of apoptosis and selectively stains nuclei of apoptotic cells as intense fluorescent blue. Thus, the morphological changes in chromatin such as condensation and fragmentation, which characterize cell apoptosis, can be readily observed [30]. In our experiments LLC cells were incubated respectively with ABT737 molecules, ZnPc-UCNPs and ABT737@ZnPc-UCNPs for 24 h, followed by laser irradiation of 980 nm at 0.40 W/cm² for 10 min and then stained with DAPI. From Fig. 4b the nuclear morphology in ABT737 group exhibited nothing

unusual. While the ZnPc-UCNPs and ABT737@ZnPc-UCNPs treated group enhanced nuclear damage. The significant difference in apoptosis between these two treated groups was further revealed by quantitative assessment (Fig. S11). ABT737@ZnPc-UCNPs increased greatly the apoptosis up to 48.5% compared with that of ZnPc-UCNPs (13.8%), suggesting better efficacy of ABT737@ZnPc-UCNPs in inducing cell apoptosis. Flow cytometry with annexin V-FITC and PI staining provided further support. Annexin V/PI staining shown in Fig. 4c indicates that treatment of ABT737@ZnPc-UCNPs induced apoptosis in 54.1% cells, much higher than 19.9% of ZnPc-UCNPs group, 5.8% of ABT737 group and 5.5% of the control group. We therefore can conclude that the ABT737@ZnPc-UCNPs improves significantly PDT efficacy.

3.3.3. ABT737@ZnPc-UCNPs mediated PDT decreased mitochondrial membrane potential ($\Delta\Psi_m$)

There is a consensus that the distinct apoptosis-induced

signals concentrate in permeability transition, leading to the dissipation of mitochondrial membrane potential (MMP, $\Delta\Psi_m$) [31–33]. According to the intracellular distribution image of ABT737@ZnPc-UCNPs (Fig. 3), the nanophotosensitizers were primarily located in mitochondria after 24 h incubation. The alteration of $\Delta\Psi_m$ were evaluated by JC-1 staining in order to identify whether the apoptosis induced by ABT737@ZnPc-UCNPs mediated PDT was associated with any effects on mitochondria. After incubation solely with ABT737, ZnPc-UCNPs and ABT737@ZnPc-UCNPs for 24 h, respectively, the cells were irradiated with NIR light at 0.40 W/cm^2 for 10 min to induce apoptosis and then stained by JC-1 dye, which is popularly used to monitor mitochondrial health because of its potential-dependent accumulation. Under 488 nm excitation, the monomer form of JC-1 (J-monomer) could be seen in the green channel (500–530 nm) and the emission shall increase when the membrane potential of mitochondria decreases. On the other hand, aggregated JC-1 (J-aggregate) in the red channel (550–600 nm) accumulated within healthy mitochondria with normal potential [34]. Serious damage of mitochondria was witnessed by the significant increase of the green emission of ABT737@ZnPc-UCNPs treated group in Fig. 4d. We also quantified the ratio of the emission intensity from J-monomer (green) to J-aggregate (red) (Fig. S12). The cells in the control group have a ratio of 0.49 ± 0.06 , whereas the ABT737@ZnPc-UCNPs treated group has the highest ratio of 2.38 ± 0.08 compared with that of 0.63 ± 0.02 for ABT737 alone group and 1.27 ± 0.05 for ZnPc-UCNPs alone group. Several lines of evidence implicated that Bcl-2 exerted a stabilizing effect on $\Delta\Psi_m$ [35]. Adding Bcl-2 inhibitor ABT737 molecules decreased lightly the $\Delta\Psi_m$. The ZnPc-UCNPs treated group exhibited a damage of mitochondria to a certain extent due to the generation of ROS. Similar decrease of $\Delta\Psi_m$ has also been observed in TiO_2 @UCNPs mediated PDT [36]. However, the drastic collapse of the $\Delta\Psi_m$ in ABT737@ZnPc-UCNPs treated group ensures that oxidative damage of ZnPc-UCNPs could be significantly aggravated by inhibition of Bcl-2.

3.3.4. ABT737@ZnPc-UCNPs mediated PDT influenced Bcl-2 family proteins

To further understand the mechanism of the apoptosis

induction by ABT737@ZnPc-UCNPs mediated PDT, the protein expression of Bcl-2 family in ABT737, ZnPc-UCNPs as well as ABT737@ZnPc-UCNPs treated LLC cells was measured by Western blot (see Experimental Section for the details). The activation of mitochondria is known to be controlled by the family of Bcl-2 proteins, which are composed of proapoptotic proteins (e.g., Bax and Bak) and antiapoptotic proteins (e.g., Bcl-2, Bcl-xL, and Mcl-1) [37]. Significant down-regulated expression of the antiapoptotic protein Bcl-2 occurred in ABT737@ZnPc-UCNPs treated group referenced to ZnPc-UCNPs group (Fig. 5a and Fig. S13), indicating an effective inhibition of Bcl-2 by ABT737 molecules. The decrease of Bcl-2 level in ZnPc-UCNPs group manifested itself that ZnPc-UCNPs mediated PDT can induce the disruption of mitochondrial function as well. In contrast, the level of the proapoptotic protein Bak increased in both ZnPc-UCNPs and ABT737@ZnPc-UCNPs treated groups. Upregulation of Bak could induce $\Delta\Psi_m$ and mitochondrial outer membrane permeability (MOMP), leading to cytochrome C release from mitochondria into the cytosol to promote cell apoptosis. As expected, the more cytochrome C released from mitochondria was observed in cells treated with ABT737@ZnPc-UCNPs compared with those treated with ZnPc-UCNPs, implying that the addition of ABT737 significantly increased the release of cytochrome C. While, in the control group or the ABT737 group, no release of cytochrome C was observed. Cytochrome C, a pivotal effector of apoptosis, can lead to the activation of caspases in the apoptosome. Caspase 3 is the main effector caspase that is involved in apoptosis [38]. ABT737 enhanced the sensitivity of cancer cells to PDT and facilitated mitochondrion-mediated apoptotic cell death as the expression of activated-caspase 3 increased significantly compared to the other groups after PDT treatment. It is known that mitochondria serve as the energy factory of the cell and the normal $\Delta\Psi_m$ is required for the maintenance of function. Notably, many more intracellular ABT737@ZnPc-UCNPs were found located in mitochondria. It is therefore inferred that ABT737@ZnPc-UCNPs contributes to the mitochondrial damage might be associated with the cells response to ABT737@ZnPc-UCNPs. The decreased mitochondrial membrane potential and the activation of mitochondrial outer membrane permeability suggest that mitochondrial damage might play a key role in response to ABT737@ZnPc-UCNPs.

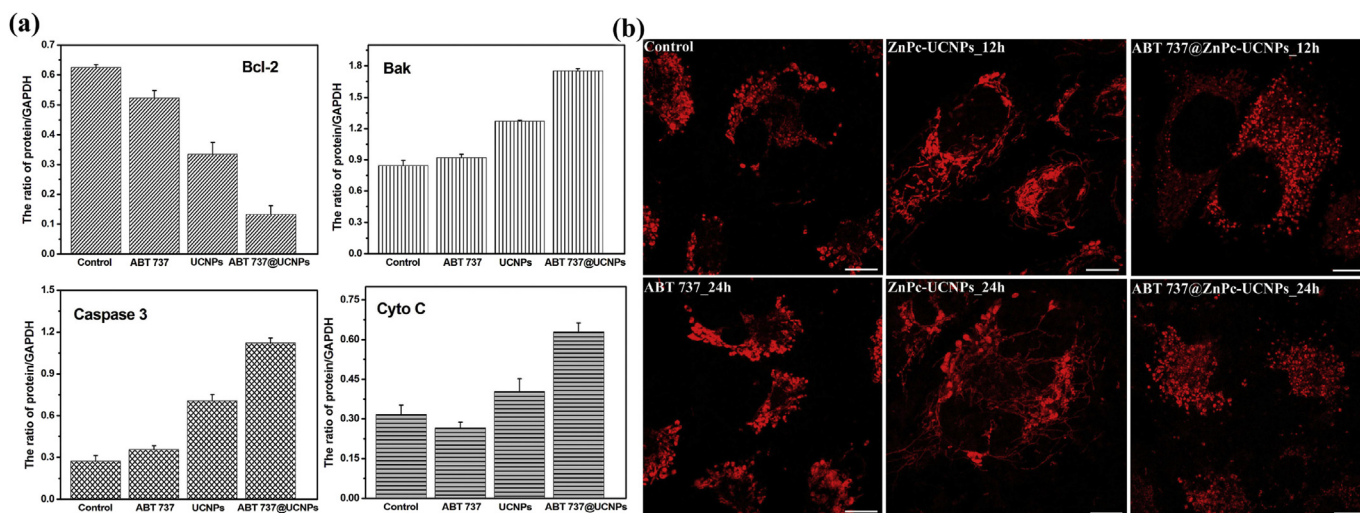


Fig. 5. (a) Representative quantitative analysis of Bcl-2, Bak, activated Caspase 3 and cytochrome C expression. After normalization with the corresponding GAPDH expression, the protein expression levels were determined using densitometry scans to obtain quantitative data. The data are expressed as the mean \pm standard deviation ($n = 3$). (b) The cells were incubated with ZnPc-UCNPs or ABT737@ZnPc-UCNPs for 12 h or 24 h at 37°C , irradiated by a 980 nm laser with dosage of 0.4 W/cm^2 for 10 min. Then the mitochondrial morphology was determined by the staining with MitoTracker Red and observed by confocal microscopy. Bar: $10 \mu\text{m}$. (For interpretation of the references to colour in this figure legend, the reader is referred to the web version of this article.)

3.3.5. ABT737@ZnPc-UCNPs mediated PDT promoted mitochondrial fission

Mitochondria in cell form a highly interconnected dynamic tubular network and undergo frequent fusion and fission, which maintains mitochondrial morphology and function. Once the balance is perturbed by apoptosis, mitochondrial tubular network goes to fragmentation. These changes are essential for downstream events of apoptosis. In order to determine if the mitochondrial fission and fusion regulate the response to ABT737@ZnPc-UCNPs mediated PDT, LLC cells were cultured with ABT737, ZnPc-UCNPs as well as ABT737@ZnPc-UCNPs for various times and followed with light irradiation, the mitochondria were then stained and measured by confocal microscopy (see Experiment Section for the details). As shown in Fig. 5b, without treatment, the normal mitochondria exhibited short tubular-like shapes in LLC cells. ABT737 treatment alone had little impact on mitochondria morphology. In the group treated with ZnPc-UCNPs for 12 h, the mitochondria elongated to longer tubules, and became hyper-fused long tubule-like shapes after 24 h. However, the mitochondria were fissured to small punctate forms in the group cultured with ABT737@ZnPc-UCNPs for 12 h, and became even smaller dots after 24 h treatment. In general, we found that ABT737 had little influence on mitochondrial morphology. ZnPc-UCNPs result in hyper-fusion of mitochondria in LLC cells in a time-dependent manner. However, ABT737@ZnPc-UCNPs could overcome ZnPc-UCNPs induced fusion and reverse to a serious fission. It is well known that mitochondrial fission sensitizes cells to apoptosis [39]. Based on our observation, we may come to the conclusion that LLC cells may adapt themselves to ZnPc-UCNPs mediated PDT through alteration of mitochondrial morphology, resulting in PDT resistance to a certain extent, and inhibition of this process by ABT737@ZnPc-UCNPs might recover the cytotoxic effect.

3.4. In vivo tumor inhibition efficacy

To evaluate the PDT effect of ABT737@ZnPc-UCNPs *in vivo*, LLC

tumor-bearing C57/6J mice were intratumorally injected with ABT737@ZnPc-UCNPs, and the tumor part was irradiated with 980 nm laser light at 0.35 W cm^{-2} for 5 min for each round, and totally 4 rounds in a course of treatment. The 980 nm irradiation dosage was only 105 J cm^{-2} for each round. The heating effect of 105 J cm^{-2} has also been tested, and the surface temperature raised only $0.1 \text{ }^\circ\text{C}$. Therefore, the light dosage used here had no serious heating effect. The groups that received intratumorally injected ABT737 and ZnPc-UCNPs followed by laser exposure with the same light dosage were taken for comparison. In addition, the groups injected with ABT737@ZnPc-UCNPs or ZnPc-UCNPs without 980 nm laser irradiation and the group without any processing were set as controls. The tumor volume in the control groups increased remarkably during the treatment (Fig. 6a). In contrast, the group treated with ZnPc-UCNPs grew more slowly and the group received injection of ABT737@ZnPc-UCNPs grew most slowly. Body weight changes can also reflect the health condition of the treated mice. As shown in Fig. S14, the body weight of mice of the control groups began to decrease from day 8 post-treatment, indicating that the living quality of the mice was affected by the tumor burden. For the ABT737@ZnPc-UCNPs treated group, their body weight gradually increased during 14 days, demonstrating that PDT treatment based on ABT737@ZnPc-UCNPs can effectively improve the survival quality of mice and prolong their lifetime. The excised tumors from these groups (Fig. 6b) confirmed the inhibition effect - the tumor size under ABT737@ZnPc-UCNPs mediated PDT treatment was much smaller than the other groups. The tumor inhibition ratio, calculated based on the tumor size, was 90.3% for ABT737@ZnPc-UCNPs group much higher than that of ZnPc-UCNPs group (59.8%), a clear evidence that ABT737 indeed enhanced the susceptibility of tumor to PDT, thus significantly increased the therapeutic efficacy of PDT.

Histological analysis of the tumors shown in Fig. 6c demonstrates a mass of aggregated neutrophils in ABT737@ZnPc-UCNPs group which is different from the control group and ABT737 group, indicating that the ABT737@ZnPc-UCNPs mediated PDT

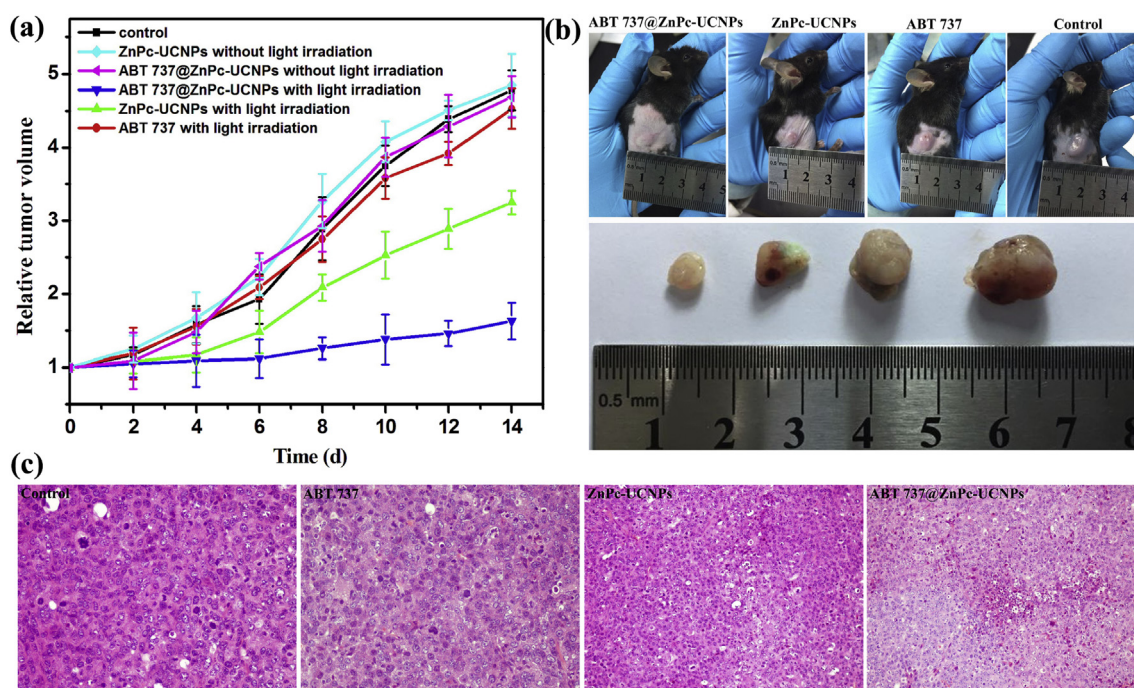


Fig. 6. (a) Tumor growth of mice in different treatment groups within 14 days. Error bars indicate standard deviations, $n = 6$. (b) Digital photographs of excised tumors from representative mice after various treatment. (c) H&E stained images of tumor sections from different treatment groups.

induced acute inflammatory reaction and systemic immunity. The generated neutrophils also facilitated the death of cancer cells [40]. Some tiny inflammatory cysts were found in ZnPc-UCNPs group, illustrating that the ZnPc-UCNPs mediated PDT also functioned, but not as efficient as the ABT737@ZnPc-UCNPs mediated one. Histological analysis was also performed in heart, liver, spleen, lung and kidney (shown in Fig. S15) and no pathological changes were observed.

3.5. Immunohistochemical analysis

In order to further investigate the ABT737@ZnPc-UCNPs mediated PDT effect on Bcl-2 family proteins *in vivo*, immunohistochemical staining for Bcl-2, Bak and Cytochrome C were carried out on tissue slices of tumors excised from the four different groups and illustrated in Fig. 7. Plenty of Bcl-2 proteins were stained in nuclei and cytoplasm as brown in color in the control, ABT737, as well as ZnPc-UCNPs groups. However, the color of Bcl-2 protein *in vivo* significantly decreased in the group with ABT737@ZnPc-UCNPs treatment, which strongly indicates that ABT737@ZnPc-UCNPs mediated PDT dramatically inhibited the expression of Bcl-2 compared with the others. In contrast, the ABT737@ZnPc-UCNPs treated group exhibited the best positive effect of pro-apoptotic protein Bak expression among all the groups (more Bak staining

in the cytoplasm). There was no significant difference in expression of Bak between the control and ABT737 groups. ZnPc-UCNPs treatment resulted in slightly more positive effect. As expected, the highest expression of Cyto C *in vivo* appeared (brown color in the cytoplasm) in ABT737@ZnPc-UCNPs treated group, in line with the result that ABT737@ZnPc-UCNPs mediated PDT caused seriously mitochondrial damage *in vitro*. It is also interesting to note that the excised tumor from ABT737@ZnPc-UCNPs treated group was less bloody than the other groups. There is a consensus that the growth of tumor is related to angiogenesis in the tumor. Bcl-2 proteins were expressed not only in tumor cells but also in vascular endothelial cells [41]. To check if the inhibition of Bcl-2 effects tumor angiogenesis, tumor microvessel density (MVD) was evaluated using immunohistochemistry for CD34. MVD can be used as a stable assessment to evaluate the therapeutic effect in tumor angiogenesis [42]. CD34 is popularly used as an endothelial cell marker of tumor vessels, which detects newly formed and preexisting big blood vessels [43]. As can be seen in Fig. 7, the expression of CD34 in ABT737@ZnPc-UCNPs treated groups was significantly decreased, indicating that MVD was reduced in tumor. In addition, the expression level of vascular endothelial growth factor (VEGF) was also detected, which is a more explicit growth factor of stimulating angiogenesis. The treatment with ABT737@ZnPc-UCNPs had a pronounced inhibitory effect on VEGF

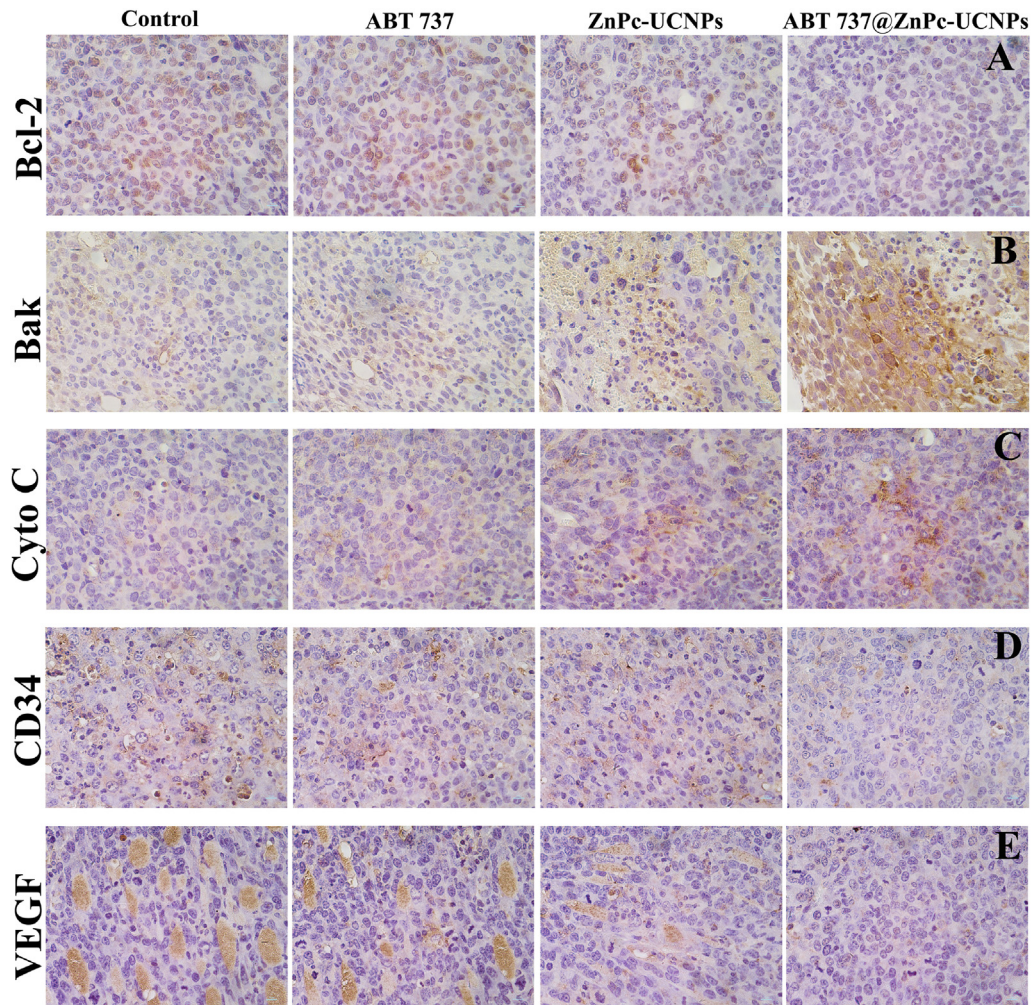


Fig. 7. Representative photographs of the tumor sections from different treatment groups examined by immunohistochemical staining for (A) Bcl-2, (B) Bak, (C) Cyto C, (D) CD34 and (E) VEGF.

in tumor compared with the other groups. All these results demonstrated that the high PDT efficacy of ABT737@ZnPc-UCNPs came not only from preventing the tumor cells survive from oxidative stimuli but also from the inhibition of tumor angiogenesis.

3.6. The tumor antioxidant environment change by ABT737@ZnPc-UCNPs *in vivo*

The ROS generated by light irradiated ABT737@ZnPc-UCNPs *in vivo* was highly toxic and reactive. However, biological systems could produce some antioxidant enzymes to combat the deleterious effects of ROS. Among many antioxidant enzymes, the reduced glutathione (GSH) together with glutathione peroxidase (GPx) and glutathione-S-transferase (GST) is known to contribute the defence against free radicals, peroxides and a wide range of xenobiotics and carcinogens [44]. To unravel the relationship between the ABT737@ZnPc-UCNPs mediated PDT and the antioxidant enzymes activity, the GSH-related enzymes were assessed in tumors excised (see the Supporting information for the details). The group without any processing was taken as control. As illustrated in Fig. 8 and Table S1, the activities of GSH and GST were significant high in control group, displaying 48.6 ± 1.2 and 35.8 ± 0.9 , respectively. No statistically significant difference in GSH, GST and GPx levels were detected between ABT737 and the control groups. The activities of GSH, GST in ZnPc-UCNPs group were slightly lower than that of the control group displaying 37.2 ± 0.6 and 26.8 ± 0.7 , respectively. While there was no significant difference in GPx levels detected between the two groups. In contrast, all the GSH-related antioxidant enzymes decreased dramatically in ABT737@ZnPc-UCNPs group especially for GSH (17.5 ± 0.3) and GST (11.4 ± 0.8). The elevation of GSH and GPx in tumor tissues may be markers of cell proliferation [45,46]. GST plays a key role in detoxifying anticancer agents, thereby preventing their cytotoxic action [47]. Many reports suggest that oxidative stress can upregulate antioxidant enzymes that render cells more resistant to succedent oxidative stimuli [48]. In our studies, all the GSH-related antioxidant enzymes exhibit extreme high levels in control and ABT737 groups, indicating its strong antioxidation ability and high cell proliferation. Although slight down-regulation of GSH and GST level was observed in the ZnPc-UCNPs treated group, the activity of GPx did not change too much compared with the control group,

manifesting that the tumor was still active to defense ROS. On the contrary, GSH-related antioxidant enzymes were significantly decreased in ABT737@ZnPc-UCNPs treated group, meaning that the tumor microenvironment of strong antioxidation was turned to be sensitive to oxidative stimuli, which holds the main responsibility for the pronounced PDT effect mediated by ABT737@ZnPc-UCNPs.

4. Conclusion

We have proposed and validated a novel strategy to effectively ease the cancer resistance to the photodynamic therapy, i.e. to integrate Bcl-2 inhibitor-ABT737 molecules into upconversion ZnPc nanophotosensitizers. The role of Bcl-2 in regulating cellular response to ABT737@ZnPc-UCNPs mediated PDT is unraveled. Inhibition of Bcl-2 not only prevents tumor cells evasion of apoptosis internally, as reflected in the decreased $\Delta\Psi_m$, the activation of MOMP, as well as the promoted mitochondrial fission, but also alters the tumor microenvironment externally, including restraining the tumor angiogenesis and reducing the levels of antioxidant enzymes, which make the tumor very susceptible to oxidative stimuli. Our study suggests that the strategy of integrating inhibiting entities with photosensitizers, exemplified by ABT737@ZnPc-UCNPs, can serve as a potential new adjuvant intervention strategy for PDT.

Acknowledgements

This work was financially supported by NSF of China (61575194, 11474278, 11674316, 11604331, 11374297). Project of Science and Technology Agency, Jilin Province (20170520113JH, 20170520112JH and 20170519002JH). Joint research program between CAS of China and KNAW of the Netherlands, European union MSCA-ITN-2015-ETN Action program, ISPIC, under grant nr. 675742, Netherlands Organisation for Scientific Research in the framework of the Fund New Chemical Innovation (2015) under grant nr.731.015.206, the 111 project (No. B13013) and John van Geuns foundation.

Appendix A. Supplementary data

Supplementary data related to this article can be found at <http://dx.doi.org/10.1016/j.biomaterials.2017.08.010>.

References

- [1] P. Agostinis, K. Berg, K.A. Cengel, T.H. Foster, A.W. Girotti, S.O. Gollnick, S.M. Hahn, M.R. Hamblin, A. Juzeniene, D. Kessel, M. Korbelik, J. Moan, P. Mroz, D. Nowis, J. Piette, B.C. Wilson, J. Golab, Photodynamic therapy of cancer: an update, *CA, Cancer J. Clin.* 61 (2011) 250–281.
- [2] Z. Huang, Y.C. Hsu, L.B. Li, L.W. Wang, X.D. Song, C.M.N. Yow, A.I. Musani, R.C. Luo, B.J. Day, Photodynamic therapy of cancer—challenges of multidrug resistance, *J. Innov. Opt. Health Sci.* 8 (2015), 1530002–1–153002–13.
- [3] M. Broekgaarden, R. Weijer, T.M. Van Gulik, M.R. Hamblin, M. Heeger, Tumor cell survival pathways activated by photodynamic therapy: a molecular basis for pharmacological inhibition strategies, *Cancer Metastasis Rev.* 34 (2015) 643–690.
- [4] M.S. Hayden, S. Ghosh, Shared principles in NF- κ B signaling, *Cell* 32 (2008) 344–362.
- [5] M. Karin, A. Lin, NF- κ B at the crossroads of life and death, *Nat. Immunol.* 3 (2004) 221–227.
- [6] P.E. Czabotar, G. Lessene, A. Strasser, J.M. Adams, Control of apoptosis by the Bcl-2 protein family: implications for physiology and therapy, *Nat. Rev. Mol. Cell. Biol.* 15 (2014) 49–63.
- [7] A. Hochman, H. Sternin, S. Gorodin, I. Korsmeyer, J. Ziv, E. Melamed, D. Offen, Enhanced oxidative stress and altered antioxidants in brains of Bcl-2-deficient mice, *J. Neurochem.* 7 (1998) 741–748.
- [8] L.M. Ellerby, H.M. Ellerby, S.M. Park, A.L. Holleran, A.N. Murphy, G. Fiskum, D.J. Kane, M.P. Testa, C. Kayalar, D.F. Bredesen, Shift of the cellular oxidation-reduction potential in neural cells expressing Bcl-2, *J. Neurochem.* 67 (1996) 1259–1267.
- [9] T. Oltersdorf, S.W. Elmore, A.R. Shoemaker, R.C. Armstrong, D.J. Augeri, An inhibitor of Bcl-2 family proteins induces regression of solid tumours, *Nature* 435 (2005) 677–681.

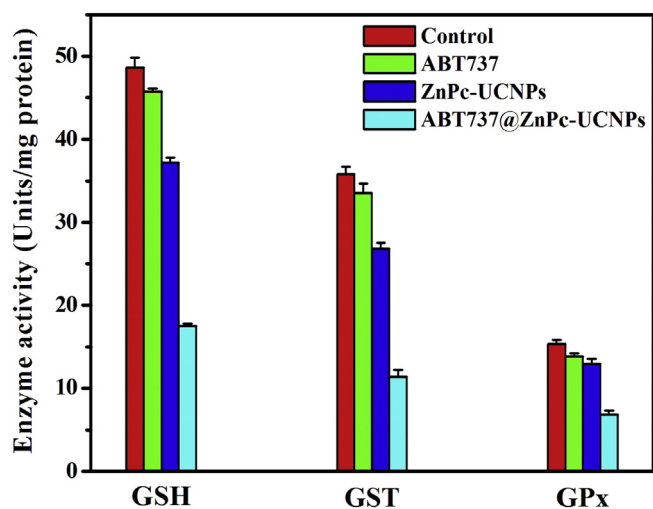


Fig. 8. Activities of GSH-related enzymes in tumor extracted from different groups. GSH, GSH reductase; GST, GSH transferase; GPx, GSH peroxidase. Means \pm SD, n = 3.

- [10] M. Tomek, T. Akiyama, C.R. Dass, Role of Bcl-2 in tumour cell survival and implications for pharmacotherapy, *J. Pharm. Pharmacol.* 64 (2012) 1695–1702.
- [11] A.V. Juarez, L.D. Sosa, A.L. De Paul, A.P. Costa, M. Farina, R.B. Leal, A.I. Torres, P. Pons, Riboflavin acetate induces apoptosis in squamous carcinoma cells after photodynamic therapy, *Journal Photochem. Photobiol. B-Biol.* 153 (2015) 445–454.
- [12] Z.J. Zhou, J.B. Song, L.M. Nie, X.Y. Chen, Reactive oxygen species generating systems meeting challenges of photodynamic cancer therapy, *Chem. Soc. Rev.* 45 (2016) 6597–6626.
- [13] Y.I. Park, K.T. Lee, Y.D. Suh, T. Hyeon, Upconverting nanoparticles: a versatile platform for wide-field two-photon microscopy and multi-modal in vivo imaging, *Chem. Soc. Rev.* 44 (2015) 1302–1317.
- [14] J. Zhou, Q. Liu, W. Feng, Y. Sun, F.Y. Li, Upconversion luminescent materials: advances and applications, *Chem. Rev.* 115 (2015) 395–465.
- [15] G. Chen, H. Qiu, P.N. Prasad, X. Chen, Upconversion nanoparticles: design, nanochemistry, and applications in theranostics, *Chem. Rev.* 114 (2014) 5161–5214.
- [16] W. Fan, W.B. Bu, J.L. Shi, On the latest three-stage development of nanomedicines based on upconversion nanoparticle, *Adv. Mater* 28 (2016) 3987–4011.
- [17] H. Dong, S.R. Du, X.Y. Zheng, G.M. Lyu, L.D. Sun, L.D. Li, P.Z. Zhang, C. Zhang, C.H. Yan, Lanthanide nanoparticles: from design toward bioimaging and therapy, *Chem. Rev.* 115 (2015) 10725–10815.
- [18] N.M. Idris, M.K.G. Jayakumar, A. Bansal, Y. Zhang, Upconversion nanoparticles as versatile light nanotransducers for photoactivation applications, *Chem. Soc. Rev.* 44 (2015) 1449–1478.
- [19] W. Zheng, P. Huang, D.T. Tu, E. Ma, H.M. Zhu, X.Y. Chen, Lanthanide-doped upconversion nano-bioprobes: electronic structures, optical properties, and biodetection, *Chem. Soc. Rev.* 44 (2015) 1379–1415.
- [20] K. Liu, X.M. Liu, Q.H. Zeng, Y.L. Zhang, X.G. Kong, Y.H. Wang, F. Cao, S.A.G. Lambrechts, M.C.G. Aalders, H. Zhang, Covalently assembled NIR nanoplatfor for simultaneous fluorescence imaging and photodynamic therapy of cancer cells, *ACS Nano* 6 (2012) 4054–4062.
- [21] F. Wang, X.G. Liu, Multicolor tuning of lanthanide-doped nanoparticles by single wavelength excitation, *Acc. Chem. Res.* 47 (2014) 1378–1385.
- [22] C. Yao, P.Y. Wang, X.M. Li, X.Y. Hu, L.Y. Wang, F. Zhang, Near-infrared-triggered azobenzene-liposome/upconversion nanoparticle hybrid vesicles for remotely controlled drug delivery to overcome cancer multidrug resistance, *Adv. Mater* 28 (2016) 9341–9348.
- [23] Y. Wang, K. Liu, X.M. Liu, K. Dohnalov, T. Gregorkiewicz, X.G. Kong, M.C.G. Aalders, W.J. Buma, H. Zhang, Critical shell thickness of core/shell upconversion luminescence nanoplatfor for FRET application, *J. Phys. Chem. Lett.* 2 (2011) 2083–2088.
- [24] E.S. Lee, H.J. Shin, K. Na, Y. Bae, Poly(L-histidine)-PEG block copolymer micelles and pH-induced destabilization, *J. Control. Release* 90 (2003) 363–374.
- [25] T. Wu, J.C. Boyer, M. Barker, D. Wilson, N.R. Branda, A “Plug-and-Play” method to prepare water-soluble photoresponsive encapsulated upconverting nanoparticles containing hydrophobic molecular switches, *Chem. Mater* 25 (2013) 2495–2502.
- [26] X.M. Liu, I. Que, X.G. Kong, Y.L. Zhang, L.P. Tu, Y.L. Chang, T.T. Wang, A. Chan, C.W.G.M. Löwik, H. Zhang, In vivo 808 nm image-guided photodynamic therapy based on an upconversion theranostic nanoplatfor, *Nanoscale* 7 (2015) 14914–14923.
- [27] J.M. Benns, J.S. Choi, R.I. Mahato, J.S. Park, S.W. Kim, pH-sensitive cationic polymer gene delivery vehicle: N-Ac-poly(L-histidine)-graft-poly(L-lysine) comb shaped polyme, *Bioconj. Chem.* 11 (2000) 637–645.
- [28] D.M. Hockenbery, Z.N. Oltvai, X.M. Yin, C.L. Milliman, S.J. Korsmeyer, Bcl-2 functions in an antioxidant pathway to prevent apoptosis, *Cell* 75 (1993) 241–251.
- [29] I. Mfouo-Tynga, H. Abrahamse, Cell death pathways and phthalocyanine as an efficient agent for photodynamic cancer therapy, *Int. J. Mol. Sci.* 16 (2015) 10228–10241.
- [30] Z.Q. Fan, H.M. Yu, N. Cui, X.G. Kong, X.M. Liu, Y.L. Chang, Y. Wu, L.K. Sun, G.Y. Wang, ABT737 enhances cholangiocarcinoma sensitivity to cisplatin through regulation of mitochondrial dynamics, *Exp. Cell Res.* 335 (2015) 68–81.
- [31] P. Marchetti, M. Castedo, S.A. Susin, N. Zamzami, T. Hirsch, A. Macho, A. Haeflner, F. Hirsch, M. Geuskens, U. Kroemer, Mitochondrial permeability transition is a central coordinating event of apoptosis, *J. Exp. Med.* 184 (1996) 1155–1160.
- [32] N. Zamzami, P. Marchetti, M. Castedo, D. Decaudin, A. Macho, T. Hirsch, S.A. Susin, P.X. Petit, B. Mignotte, G. Kroemer, Sequential reduction of mitochondrial transmembrane potential and generation of reactive oxygen species in early programmed cell death, *J. Exp. Med.* 182 (1995) 367–377.
- [33] X. Liu, C.N. Kim, J. Yang, R. Jemerson, X. Wang, Induction of apoptotic program in cell-free extracts: requirement for dATP and cytochrom C, *Cell* 86 (1996) 147–157.
- [34] X.M. Zhang, F.J. Ai, T.Y. Sun, F. Wang, G.Y. Zhu, Multimodal upconversion nanoplatfor with a mitochondria-targeted property for improved photodynamic therapy of cancer cells, *Inorg. Chem.* 55 (2016) 3872–3880.
- [35] S. Shimizu, Y. Eguchi, W. Kamiike, S. Waguri, Y. Uchiyama, H. Matsuda, Y. Tsujimoto, Bcl-2 blocks loss of mitochondrial membrane potential while ICE inhibitors act at a different step during inhibition of death induced by respiratory chain inhibitors, *Oncogene* 13 (1996) 21–29.
- [36] Z.Y. Hou, Y.X. Zhang, K.R. Deng, Y.Y. Chen, X.J. Li, X.R. Deng, Z.Y. Cheng, H.Z. Lian, C.X. Li, J. Lin, UV-emitting upconversion-based TiO₂ photosensitizing nanoplatfor: near-infrared light mediated in vivo photodynamic therapy via mitochondria-involved apoptosis pathway, *ACS Nano* 9 (2015) 2584–2599.
- [37] M.F. Delft, A.H. Wei, K.D. Mason, C.J. Vandenberg, L. Chen, P.E. Czabotar, S.N. Willis, C.L. Scott, C.L. Day, S. Cory, J.M. Adams, A.W. Roberts, D.C.S. Huang, The BH3 mimetic ABT-737 targets selective Bcl-2 proteins and efficiently induces apoptosis via Bak/Bax if Mcl-1 is neutralized, *Cancer Cell.* 10 (2006) 389–399.
- [38] S.S. Agrawal, S. Saraswati, R. Mathur, M. Pandey, Cytotoxic and antitumor effects of brucine on ehrlich ascites tumor and human cancer cell line, *Life Sci.* 89 (2011) 147–158.
- [39] C. Sheridan, S.J. Martin, Mitochondrial fission/fusion dynamics and apoptosis, *Mitochondrion* 10 (2010) 640.
- [40] K.L. Singel, B.H. Segal, Neutrophils in the tumor microenvironment: trying to heal the wound that cannot heal, *Immunol. Rev.* 273 (2016) 329–343.
- [41] L.X. Liao, M.B. Zhao, X. Dong, Y. Jiang, K.W. Zeng, P.F. Tu, TDB protects vascular endothelial cells against oxygen-glucose deprivation/reperfusion-induced injury by targeting miR-34a to increase Bcl-2 expression, *Sci. Rep.* 6 (2016) 37959.
- [42] S.G. Priyadarshini, D. Basu, R. Kar, T.K. Dutta, Proliferation and angiogenesis using immunohistochemistry in prognosticating multiple myeloma, *Indian J. Hematol. Blood Transfus.* 32 (2016) 418–423.
- [43] R. Kumaraguruparana, R. Subapriya, P. Viswanathan, S. Nagini, Tissue lipid peroxidation and antioxidant status in patients with adenocarcinoma of the breast, *Clin. Chim. Acta* 325 (2002) 165–170.
- [44] C.R. Yang, Y.C. Ou, J.H. Kuo, Y.L. Kao, C.L. Chen, S.Y. Yean, Intracellular glutathione content of urothelial cancer in correlation to chemotherapy response, *Cancer Lett.* 119 (1997) 157–162.
- [45] E. Obrador, J. Navarro, J. Mompo, M. Asensi, J.A. Pellicer, J.M. Estrela, Glutathione and the rate of cellular proliferation determine tumor cell sensitivity to tumor necrosis factor in vivo, *Biochem. J.* 325 (1997) 183–189.
- [46] J.H. Doroshow, Glutathione peroxidase and oxidative stress, *Toxicol. Lett.* 82 (1995) 395–398.
- [47] A. Matsui, T. Ikeda, K. Enomoto, Increased formation of oxidative DNA damage, 8-Hydroxy 2'-Deoxyguanosine, in human breast cancer tissue and its relationship to GSTP1 and COMT genotypes, *Cancer Lett.* 151 (2000) 87–95.
- [48] B. Halliwell, The antioxidant paradox, *Lancet* 355 (2000) 1179–1180.